EBioMedicine 45 (2019) 328–340

Contents lists available at ScienceDirect

EBioMedicine

journal homepage: www.ebiomedicine.com

EBioMedicine
Published by THE LANCET

TLR9 agonist MGN1703 enhances B cell differentiation and function in lymph nodes

Mariane H. Schleimann [a,b,*], Maria-Louise Kobberø [c], Line K. Vibholm [a,c], Kathrine Kjær [a,c], Leila B. Giron [d], Kathleen Busman-Sahay [b], Chi Ngai Chan [b], Michael Nekorchuk [b], Manuel Schmidt [e], Burghardt Wittig [e,f,1], Tine E. Damsgaard [c,g], Peter Ahlburg [h], Michel B. Hellfritzsch [c,i], Kaja Zuwala [a,c], Frederik H. Rothemejer [c], Rikke Olesen [c], Phillipp Schommers [j,k,l], Florian Klein [j,l], Harsh Dweep [m], Andrew Kossenkov [m], Jens R. Nyengaard [c,n], Jacob D. Estes [b], Mohamed Abdel-Mohsen [d], Lars Østergaard [a,c], Martin Tolstrup [a,c], Ole S. Søgaard [a,c], Paul W. Denton [a,c,**]

[a] Department of Infectious Diseases, Aarhus University Hospital, Denmark
[b] Vaccine and Gene Therapy Institute, Oregon Health and Science University, Portland, OR, USA
[c] Department of Clinical Medicine, Aarhus University, Denmark
[d] Vaccine & Immunotherapy Center, The Wistar Institute, Philadelphia, PA, USA
[e] Mologen AG, Berlin, Germany
[f] MolBio2Math - Molecular Biology & Integral Biomathics, a non-profit Foundation Institute, Berlin, Germany
[g] Department of Plastic and Breast Surgery, Plastic Surgery Research Unit, Aarhus University Hospital, Denmark
[h] Department of Anesthesiology, Aarhus University Hospital, Denmark
[i] Department of Radiology, Aarhus University Hospital, Denmark
[j] Institute of Virology, Faculty of Medicine and University Hospital of Cologne, University of Cologne, 50931 Cologne, Germany
[k] Department of Internal Medicine, Faculty of Medicine and University Hospital Cologne, University of Cologne, 50931 Cologne, Germany
[l] German Center for Infection Research, Partner Site Bonn-Cologne, 50931 Cologne, Germany
[m] Bioinformatics Facility, The Wistar Institute, Philadelphia, PA, USA
[n] Core Centre for Molecular Morphology, Section for Stereology and Microscopy, Department of Clinical Medicine, Centre for Stochastic Geometry and Advanced Bioimaging, Aarhus University Hospital, Aarhus, Denmark

ARTICLE INFO

Article history:
Received 1 May 2019
Received in revised form 27 June 2019
Accepted 2 July 2019
Available online 9 July 2019

Keywords:
HIV cure
TLR9 agonist
B cell differentiation
B cell follicle
Antibody glycosylation

ABSTRACT

Background: TLR9 agonists are being developed as immunotherapy against malignancies and infections. TLR9 is primarily expressed in B cells and plasmacytoid dendritic cells (pDCs). TLR9 signalling may be critically important for B cell activity in lymph nodes but little is known about the in vivo impact of TLR9 agonism on human lymph node B cells. As a pre-defined sub-study within our clinical trial investigating TLR9 agonist MGN1703 (lefitolimod) treatment in the context of developing HIV cure strategies (NCT02443935), we assessed TLR9 agonist-mediated effects in lymph nodes.
Methods: Participants received MGN1703 for 24 weeks concurrent with antiretroviral therapy. Seven participants completed the sub-study including lymph node resection at baseline and after 24 weeks of treatment. A variety of tissue-based immunologic and virologic parameters were assessed.
Findings: MGN1703 dosing increased B cell differentiation; activated pDCs, NK cells, and T cells; and induced a robust interferon response in lymph nodes. Expression of Activation-Induced cytidine Deaminase, an essential regulator of B cell diversification and somatic hypermutation, was highly elevated. During MGN1703 treatment IgG production increased and antibody glycosylation patterns were changed.
Interpretation: Our data present novel evidence that the TLR9 agonist MGN1703 modulates human lymph node B cells in vivo. These findings warrant further considerations in the development of TLR9 agonists as immunotherapy against cancers and infectious diseases.

* Correspondence to: M. H. Schleimann, Postdoc at Research Department of Infectious Diseases, Aarhus University Hospital, Skejby, Palle Juul Jensens Boulevard 99, 8200 Aarhus, Denmark.
** Correspondence to: P. W. Denton University of Nebraska at Omaha, Allwine Hall 109B, 6001 Dodge Street, Omaha, NE 68182-0040, USA.
E-mail addresses: Marsch@rm.dk (M.H. Schleimann), pdenton@unomaha.edu (P.W. Denton).
[1] Senior advisor to Mologen AG, Berlin, Germany.

https://doi.org/10.1016/j.ebiom.2019.07.005

Fund: This work was supported by Aarhus University Research Foundation, the Danish Council for Independent Research and the NovoNordisk Foundation. Mologen AG provided study drug free of charge.

1. Introduction

Pattern recognition receptors are innate molecules that sense pathogen-associated or danger-associated molecular patterns [1]. One such receptor, the *toll*-like receptor 9 (TLR9), is found primarily in endosomes of plasmacytoid dendritic cells (pDCs) and B cells where it detects non-methylated cytosine-guanine (CpG) DNA motifs [2,3]. These dinucleotide motifs are frequently found in bacterial DNA as well as in transformed cells [1–4]. The downstream effects of TLR9 stimulation in human pDCs are well described ex vivo and in vivo [1–8]. In short, TLR9 stimulated pDCs produce interferon α (IFN-α). This type I interferon production leads to a stimulatory environment that results in T, NKT, and NK cells becoming activated with improved capacity for cytotoxic effector functions. Since engaging TLR9 leads to heightened activity of immune effector cells, the development of TLR9 agonists as immunotherapy for cancers and infectious diseases is a field of intense research.

TLR9 agonists include multiple classes of CpG DNA oligonucleotides (CpG ODNs) as well as members of the double stem loop immunomodulator (dSLIM) class of molecules [2,4]. CpG ODNs are linear DNA fragments that harbor CpG motifs and these fragments are typically protected from nuclease degradation by a modified phosphorothioate backbone. To avoid chemical modification leading to unwanted side effects, the dSLIM molecules utilize a covalently-closed dumbbell-shaped configuration offering protection from nucleases. Because the major effects of TLR9 stimulation occur in lymphoid tissue, we need to study this specific anatomical compartment to fully understand how TLR9 agonists engage the immune system. Such investigations provide profound insights into how responses to TLR9 agonism differ between anatomical compartments. For example, we previously reported compartmentalized human intestinal responses to MGN1703 (lefitolimod; a member of the dSLIM class of TLR9 agonists [4,9–11]) dosing that were quite nuanced and limited to a type I interferon response [6]. This was distinct from findings in peripheral blood, which revealed that these same individuals mounted both type I and type II interferon responses [6]. In comparison to the immune effector functions that occur in intestines, lymph nodes function primarily as inductive sites for adaptive immune responses. Improved antibody maturation and function are key among the essential adaptive immune responses that are manifested in lymph node follicles [12]. B cell follicles can be found either as primary follicles or secondary follicles. When an antigen stimulates a B cell, the B cell acquire the ability to migrate into primary follicles, where the B cells receive signals from follicular dendritic cells and T follicular helper cells to proliferate and form a germinal center. This formation of a germinal center creates a secondary follicle. In the secondary follicle the B cells undergo somatic hypermutation, affinity maturation and selection for differentiation into memory B cells or plasma cells [12,13].

B cells and plasma cells express TLR9 [14], however, knowledge on how TLR9 signalling affects human peripheral B cells is incomplete and the impact of TLR9 agonist treatment on human lymph node B cells is unknown. Ex vivo and in vivo murine studies as well as ex vivo human B cell studies have shown that TLR9 agonism promotes B cell differentiation and proliferation, which is accompanied by immunoglobulin class switching and antibody production [15–21]. Interestingly, in small-cell lung cancer patients presence of activated B cells have shown a predictive value for overall survival in a small patient population, which points to the importance of a further evaluation of B cell populations [10]. Thus, it remains an open question how TLR9 agonism impacts human B cell differentiation and function in vivo [22]. Furthermore, it is unknown whether peripheral blood outcomes of TLR9 stimulation mirror the impacts of TLR9 agonist treatment in lymph nodes. To answer these important questions, we examined lymph nodes alongside with paired peripheral blood samples at baseline and during MGN1703 administration in a clinical trial among HIV patients.

Research in context

Evidence before this study

Synthetic TLR9 agonists are being developed as immunotherapy for the treatment of cancers and chronic infections as well as vaccine adjuvants. Few human PBMC in vitro or murine in vivo studies have examined the direct effect of TLR9 agonists on B cells. Although the analyses utilized in these studies were not designed for in depth interrogation of B cells, they indicated that B cell proliferation and differentiation are stimulated by TLR9 agonism. However, no previous studies have investigated the in vivo TLR9 agonist impact on B cells in human lymph nodes. A trio of papers reported that local application of a TLR9 agonist at the site of melanoma resection was sufficient to induce dendritic cell and cytotoxic T cell activation in sentinel lymph nodes. Collectively, the literature on TLR9 agonist impact on human B cells differentiation and function is very limited.

Added value of this study

Here we present an unprecedented longitudinal study of lymph node biology across 24 weeks of TLR9 agonist therapy in humans. We also provide novel evidence that TLR9 agonist treatment readily modulates human B cell population dynamics in vivo. The study population consists of HIV-infected individuals who continued suppressive standard-of-care antiretroviral therapy throughout the duration of TLR9 agonist treatment. Thus, we do not only offer novel insights into basic lymph node biology during TLR9 agonist treatment, but we also present data on HIV persistence in lymph nodes from a large cohort of paired lymph node samples.

Implications of all the available evidence

Our data demonstrates that TLR9 agonism promotes B cell differentiation and leads to increased levels of antibodies, which exhibit altered glycosylation patterns. Specific TLR9 agonist-modulated glycosylation changes were associated with reductions in the amount of HIV that persists during standard-of-care antiretroviral therapy. The new knowledge presented here has immediate value for the design and conduct of interventional trials utilizing TLR9 agonist immunotherapy for oncology and infectious diseases.

2. Materials and methods

2.1. Study design and participants

Fourteen HIV-1 infected individuals on long-term cART were enrolled in the TEACH-B study (Toll-like receptor 9 enhancement of antiviral immunity in chronic HIV-1 infection part B: an investigator initiated single-arm, phase Ib/IIa clinical trial; ClinicalTrials.gov ID: NCT02443935) [8]. Twelve participants completed the study. The study was approved by the National Health Ethics Committee, Denmark (#1–10–72-10-15) and the Danish Medical and Health Authorities (#2015014125). Each participant provided written informed consent before any study activities. During the interventional phase of TEACH-B, participants continued to take cART as they received two bilateral subcutaneous injections of 60 mg MGN1703 [lefitolimod; Mologen AG, Berlin, Germany] two times per week for 24 weeks (Fig. 1a). MGN1703 injections were either in each side of the abdomen or in each upper thigh.

2.2. Lymph node harvest and processing

Of the fourteen individuals eight participants consented to have a lymph node excision at baseline and during the last week of treatment (week 24) (Fig. 1a). Upon ultrasonic verification of the lymph node localized laterally to the superficial circumflex iliac artery, the lymph node was marked on the skin. Lymph nodes from baseline and during week 24 were taken from either side. The lymph node was excised using ultrasonography guided electrocautery. Immediately after excision, ~20% of the lymph node was placed in 10% NBF for 24 h and then paraffin embedded. Non-fixed lymph node tissues were stored on ice in "suspension media" (i.e. PBS supplemented with 0·5% BSA, 1% Pen/Strep and excess DNase) for transport. Once in the laboratory, lymph node tissues were immediately processed to isolate lymph node mononuclear cells (LNMC). LNMC were extracted via mechanical disruption, washed in suspension media and strained through a 70 μm cell strainer. The lymph node wash supernatant was saved and stored at -80 °C for antibody glycosylation analysis. LNMC were analysed fresh by flow cy-

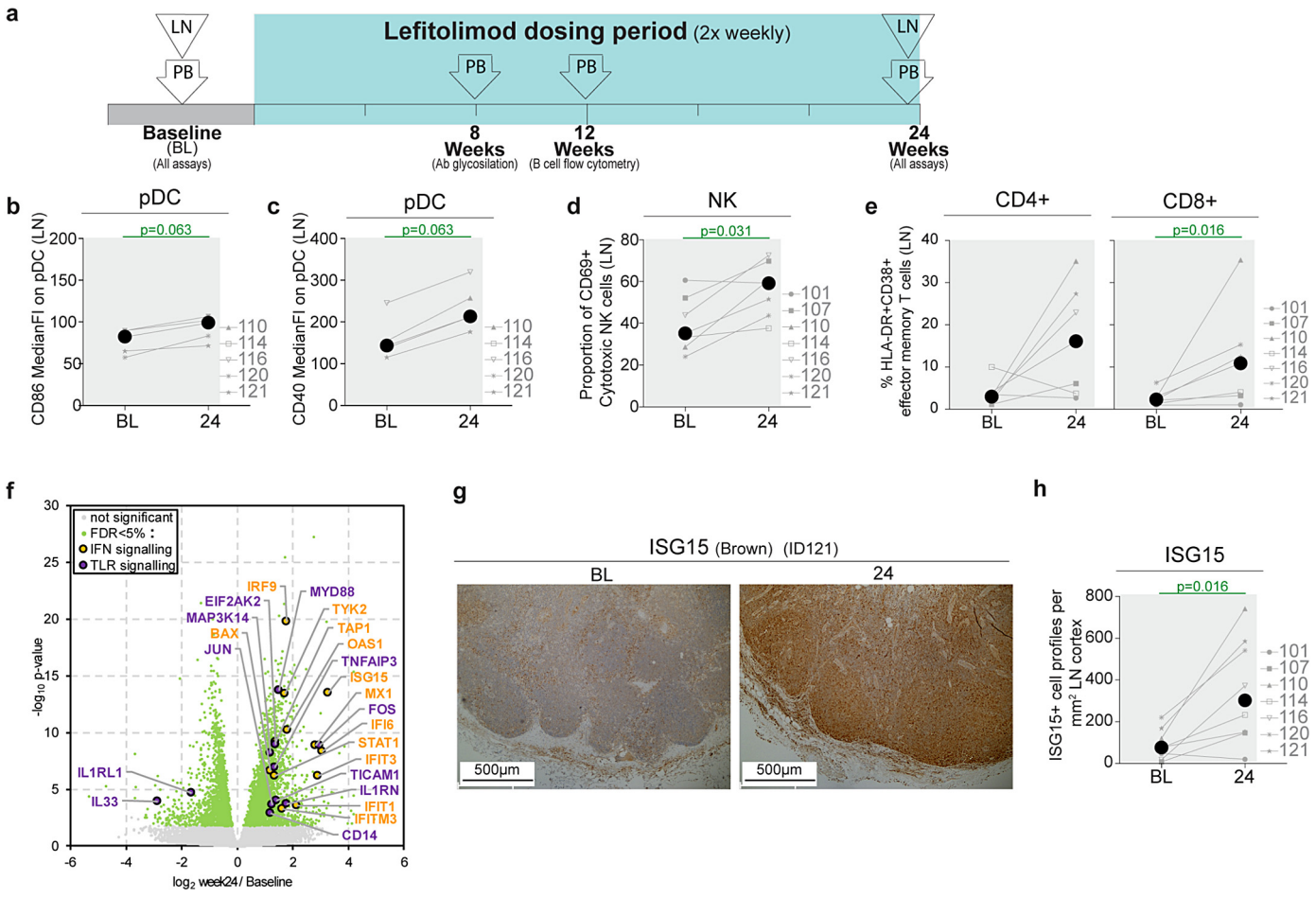

Fig. 1. MGN1703 treatment activates lymph node plasmacytoid dendritic, natural killer cells and T cells. (a) Study outline of MGN1703 dosing and sample collection time points. During the intervention the study participants continued cART treatment. (b-c) Proportions of lymph node pDC expression levels of CD86 (B) and CD40 (C) are shown. Additional pDC data are presented in Fig. S1a. (d) Proportions of lymph node CD69 positive cytotoxic NK cells (CD3−/CD56dim/CD16+) are shown. Additional NK cell data are presented in Fig. S1b. (e) Proportions of activated (HLA-DR+/CD38+) lymph node effector memory (CCR7−/CD45RA−) CD4+ (left) and CD8+ (right) T cells are shown. Additional T cell data are presented in Fig. S1c-e. (f) Volcano plot highlighting *p*-values and the MGN1703-induced fold changes from week 24 to baseline of genes related to Interferon [IFN (orange)] and Toll-like Receptor [TLR (purple)] signalling. MGN1703 regulated transcripts with an FDR < 5% is highlighted. Multiple comparisons accounted for as described in the methods. (g-h) Example baseline and on treatment (week 24) immunohistochemistry stains for ISG15 protein are shown (g). This stain was performed prior to direct inspection quantitation of the numbers of ISG15 positive cell profiles in the lymph node cortex reported in (h). Statistics: Wilcoxon matched-pairs signed-rank test (b-e;h). Axis time notations: baseline (BL) and 24 weeks (24). The n value for each analysis is defined via individual participant data points, which are graphed with grey symbols/lines and defined in adjacent legends or individually labelled in correlation plots. Black circles represent median points.

tometry as described below or lysed and preserved at -80 °C in RLT+ buffer (Allprep isolation kit, Qiagen #80204, Germantown, MD) for PCR to detect viral nucleic acids and RNASeq analyses. For some of the lymph nodes there was not sufficient amount of tissue to do all the analyses and we had to prioritize which analyses were performed. Lymph nodes that were analysed will be noted with labels in each Figure.

2.3. Flow cytometry

Flow cytometry analyses were performed on red blood cell (RBC)-lysed peripheral blood leukocytes (15 min at room temperature in 1× RBC lysis buffer, Biolegend, CA, USA) (baseline, week 12 and week 24) or freshly isolated LNMC (baseline and week 24) (Fig. 1a). For all stains, Fc-receptors were blocked with Human Trustain FcX blocking buffer for 5 min at 4 °C (BioLegend, CA, USA). Cells were mixed with antibodies in BD Horizon™ Brilliant Stain Buffer (BD Biosciences, USA) and incubated in the dark for 20 min at 4 °C, then washed twice in PBS + 2% FBS). The size of plasma blasts was estimated based on median forward scatter values for the gated population. All sample data were acquired on a FACSVerse (BD Biosciences, USA) and analyses were performed using FlowJo software (v. 10·0·8r1) [Research Resource Identifier (RRID): SCR_008520] (Treestar, Inc., OR, USA). List of antibodies is presented in Table S1.

2.4. RNA sequencing

Cellular RNA was purified using the AllPrep DNA/RNA kit (Qiagen, Ventura CA) as specified by the manufacturer. RNA quality was validated using the Agilent TapeStation, and the High Sensitivity RNA Screentape (Agilent, Santa Clara, CA) and quantity was determined using the Qubit 2·0 Fluorometer (ThermoFisher Scientific, Waltham, MA). cDNA was generated from 10 ng of total RNA using the SMART-Seq v4 Ultra Low Input RNA Kit for Sequencing (Takara Bio USA, Inc., Mountain View, CA) according to manufacturer's directions. Then, 150 pg of the cDNA was used to prepare library for Illumina sequencing using the Nextera XT Library Prep Kit (Illumina, San Diego, CA) according to manufacturer's directions. Overall library size was determined using the Agilent TapeStation and the DNA High Sensitivity 5000 Screentape (Agilent, Santa Clara, CA). Equimolar number of libraries were pooled, denatured and High-Output, Single-Read, 36/38 base pair paired end Next Generation Sequencing was done on a NextSeq 500 (Illumina, San Diego, CA).

2.5. RNASeq analysis

RNA-seq data was aligned using *bowtie2* against hg38 version of the human genome and *RSEM* v1.2.12 software was used to estimate raw read counts and RPKM using Ensemble transcriptome information. *DESeq2* was used to estimate significance of differential expression between two groups [23–25]. Genes with expression changes passing FDR < 5% threshold changed at least two fold were considered significant. Gene set enrichment analysis was done using QIAGEN's Ingenuity® Pathway Analysis software (IPA®, QIAGEN Redwood City, www.qiagen.com/ingenuity; RRID:SCR_008653) using "Canonical pathways" categories. Select pathways that passed $p < .05$ significance threshold and had at least 5 significantly changed genes were reported. The abundance of cell types was estimated using CIBERSORT software (RRID:SCR_016955) [26]. The CIBERSORT analysis was performed on RNAseq DESeq2-normalized read counts without quantile normalization in relative and absolute modes. Significance of changes in cell type abundance between treated and untreated patients was tested using paired *t*-test and results with $p < .05$ were considered significant. Correlation of RNAseq DESeq2-normalized read counts was done using Pearson correlation and nominal *p*-values were adjusted for multiple testing using Benjamini-Hochberg procedure [27].

2.6. Immunohistochemistry (IHC)

IHC was performed on formalin-fixed paraffin-embedded (FFPE) 4–5 μm serial sections as previously described [28]. Briefly, sections were deparaffinized and rehydrated followed by heat-induced epitope retrieval (HIER) performed with Citrate buffer pH 6·0 (Sigma-Aldrich) or Citraconic Anhydride buffer (details are provided in Table S2. When necessary, blocking was performed with 1% Casein in TBS (ThermoFisher Scientific,) for 30 min at room temperature. Subsequently, the sections were incubated with optimized concentrations of unconjugated primary antibodies diluted in blocking buffer (1% Casein) for 1 h at room temperature or overnight at 4 °C. Thereafter, the sections were washed and incubated with 3% H_2O_2 to block endogenous peroxidases, followed by detection of primary antibody with an appropriate Polink-1 or Polink-2 polymer detection kit (GBI Labs) conjugated with Horseradish Peroxidase or Alkaline phosphatase. Between each step, the sections were washed three times with 1× TBS-Tween20. To visualize the sites of antigen expression, ImmPACT DAB (3,3′-diaminobenzidine) Substrate (Vector Laboratories) or Warp Red ™ (Biocare Medical) was added for 2 min at room temperature. Finally, sections were counterstained with Hematoxylin, for Warp Red developed slides covered with ClearMount (diluted 1:5 in ddH20; Invitrogen), dried for 60 min at 60 °C or overnight at 40 °C, and all slides were mounted with Permount (Electron Microscopy Sciences) and scanned at high magnification (x200) using the Aperio AT2 System (Leica Biosystems) yielding high-resolution data from the entire tissue section. List of primary antibodies and conditions is provided in Table S2. The number of ISG15 positive cells was quantified as previously described [6,29]. The frequency of CD4 (DAB) positive cells was quantified using FIJI version 2·0·0-rc68/1·52i. After color deconvolution (FastRed, FastBlue, DAB) the threshold for DAB was evaluated and set to 100.

2.7. Immunofluorescent (IF) assays

IF stains were performed to assess the impact of MGN1703 on B cell follicle maturation. In total 56 sections of 5 μm each were assessed (i.e.7 participants × 2 time points x 4 sections per time point where the 4 sections were serially cut with 25 μm distance between assayed sections). Primary and secondary B cell follicles were visualized using anti-CD4, anti-CD20, and anti-IgD antibodies. IF was performed on formalin-fixed paraffin-embedded (FFPE) 5 μm serial sections. Sections were deparaffinized and rehydrated followed by heat-induced epitope retrieval (HIER) performed with Citraconic Anhydride (CA) buffer (details are provided in Table S2). After HIER the tissue was left in the CA buffer to cool at RT for 20 min followed by a 10 min wash in dH_2O. Then they were washed in 0·1% TBS-Tween20 before incubating with anti-IgD at 4 °C overnight. Thereafter, the sections were washed and incubated with 1·5% H_2O_2 to block endogenous peroxidases. Then, sections were incubated with a Polink-2 Rabbit polymer kit conjugated with Horseradish Peroxidase (HRP) (GBI-labs). Between each step, the sections were washed 10 min with 0·1% TBS-Tween20. To visualize the sites of antigen expression Tyramide signal amplification (TSA) reagent conjugated with Alexa Fluor™488 was added in a 1:500 dilution for 10 min. Before incubating the slide with anti-CD20 antibody overnight at 4 °C the sections were microwaved at power level 10 for 1 min followed by 15 min at power level 2, cooled for 10 min, washed twice with dH_2O and washed once with 0·1% TBS-Tween20. Anti-CD20 antibody stain was visualized using a Polink-2 Mouse polymer kit conjugated with Horseradish Peroxidase and TSA reagent conjugated with Alexa Fluor™647. Finally, after a second round in the microwave as described above, CD4 was detected by incubating primary anti-CD4 antibody for 1 h at RT followed by secondary anti-Rabbit antibody conjugated with Alexa Fluor™594 (RRID: AB_2534073). DNA was visualized with DAPI (Invitrogen) 1:25,000 for 10 min. To prevent autofluorescence, sections were incubated with filtered Sudan Black (diluted 10:1 in 10xTBS) for 20 min, washed and mounted with Prolong Gold anti-fade mounting

media. Sections were imaged using a Keyence BZ-X710 at 20× (Nikon Plan Apo; NA 0·75) and stitched using Keyence software, and primary and secondary follicles were manually counted. Primary B cell follicles were defined if the germinal center was IgD positive, whereas secondary B cell follicles were IgD negative in the germinal center. All tissue sections were analysed and subsequently top and bottom of secondary follicle that initially was characterized as a primary follicle was corrected and counted as a secondary follicle when detected as such on another section.

2.8. Plasma IgG quantification

Total IgG as well as IgG1, IgG2, IgG3 and IgG4 plasma levels were determined at the Clinical Biochemistry Lab at Aarhus University Hospital, Aarhus, Denmark.

2.9. Glycan analysis

Lymph node wash was concentrated using Amicon Ultra-4 Centrifugal Filter Unit (Millipore Sigma). Total IgG was purified from plasma and concentrated lymph node wash using Pierce™ Protein G Spin Plate for IgG Screening (Thermo Fisher). IgGs from lymph node wash was concentrated using Amicon Ultra-0·5 Centrifugal Filter Unit (Millipore Sigma). *N*-glycans were released using peptide-N-glycosidase F (PNGase F) and labelled with 8-aminopyrene-1,3,6-trisulfonic acid (APTS) using the GlycanAssure APTS Kit (Thermo Fisher), following the manufacturer's protocol. Labelled *N*-glycans were analysed using the 3500 Genetic Analyzer capillary electrophoresis system. Relative abundance of IgG glycan structures was quantified by calculating the area under the curve of each glycan structure divided by the total glycans.

2.10. Antibody neutralization assay: protocols for neutralizing antibody assay

Our protocols for production and titration of Env-pseudotyped viruses and neutralizing antibody assays are adapted from protocols from David C. Montefiori lab: https://www.hiv.lanl.gov/content/nab-reference-strains/html/home.htm [30].

2.11. Antibody neutralization assay: cell culture

HEK-293 T cells and TZM-bl cells (obtained though NIH AIDS Reagents Programme (Cat#8129) from Dr. John C. Kappes, and Dr. Xiaoyun Wu [31–35];) were cultured in complete DMEM (cDMEM) that is: DMEM (Gibco #11960–044) + 10% FCS + 2 mM L-Glutamine (Thermo # 25030024) + 1 mM Sodium Pyruvate (Gibco# 11360–070) + 50 μg/mL Gentamicin (Sigma # G1397-10ML) + 20 mM HEPES (Biochrom # L1613).

2.12. Antibody neutralization assay: luciferase reporter gene assay

TZM-bl cells were incubated with the virus for 48 h. For development a luciferin/lysing-agent (10 mM MgCl2 (Sigma #M8266)), 0.3 mM ATP (Sigma #A2383), 0.5 mM Coenzyme A (Sigma #C3144), 1 mM D-Luciferin (Zellbio # LUCNA), and 17 mM IGEPAL (Sigma# I8896) in Tris-HCL was added to all wells. After 2 min the supernatant was transferred to a new black 96-well plate (Corning #CLS3915) and the relative light units (RLUs) were detected on a luminometer.

2.13. Antibody neutralization assay: production and titration of Env-pseudotyped viruses

A Panel of twelve global HIV-1 Env clones was used that represents the major genetic subtypes and circulating recombinant forms of HIV-1 [36]. Twelve plasmids encoding envelopes and a backbone plasmid (pSG3deltaENV NIH AIDS Reagents Programme #11051) were expanded in STBL3 bacteria at 37 °C for 16 h and then purified using MidiPrep kit (MachereyNagel). Control pseudovirus encoding envelope from murine leukaemia virus (MLV) was expanded in the same way. 293 T cells were seeded on T75 flasks at such a density that after 24 h of culture they reached 60–90% confluency. When cells reached confluency, they were transfected with 4 μg of plasmid encoding envelope and 8 μg of backbone plasmid using Fugene HD (Promega Cat#E2311). After 3 h media was exchanged and the cells were incubated for the next 24 or 48 h when the supernatants with pseudoviruses were collected, filtered through 0.45 μm filter, aliquoted and stored at -80 °C. Env-pseudotyped viruses were titrated by preparing serial dilutions on 96-well plate in cDMEM. TZM-bl cells resuspended in cDMEM containing 10 μg/mL DEAE dextran were seeded on a plate with pseudoviruses dilutions and incubated for 48 h. We performed luciferase assay to calculate virus titer. Minimum level of infectivity had to have the luminescence signal at least 10 times higher than the cell control wells but not high enough to cause cytotoxicity.

2.14. Antibody neutralization assay: readout

Plasma from the patients was inactivated at 56 °C for 45 min. 0·5 mL of plasma was mixed with 14 mL of PBS and 250 μL of Protein G sepharose 4 Fast Flow (GE Healthcare Cat#17–0618) and incubated with rotation overnight at 4 °C. Samples were spun at 1250 rpm for 5 min, supernatants were removed and protein G sepharose with bound IgG was applied onto poly-prep chromatography column (Biorad Cat#7311550). The column was washed three times with PBS. IgG was eluted from the column with 2 mL of 0·1 M glycine pH 3 (AlfaAesar, Cat#J62527). Solution was neutralized with Tris pH 8·0. Buffer was exchanged to PBS on Amicon ultra-4 centrifugal unit ultracel 30 (SigmaAldrich Cat# Z740192). IgG concentration was measured on Nanodrop Denovix DS11FX. Serial dilutions of IgG from each patient were incubated with appropriate dilution of Env-pseudoviruses on 96-well plates for 60 min. After 60 min TZM-bl cells in cDMEM with 10 μg/mL of DEAE dextran were seeded on the plates with IgG and Env-pseudoviruses. 48 h later we performed luciferase assay and calculated antibody neutralization as IC50 (μg/mL).

2.15. Cell-associated HIV-1 DNA and unspliced HIV-1 RNA

We used digital droplet PCR (ddPCR) to quantify HIV-1 nucleic acid levels in LNMC. Template preparation and denaturation were performed as previously described [37]. Primers and probes are listed in Table S3. Samples were assayed in triplicates for HIV-1 DNA and duplicate for the RPP30 reference gene. Unspliced HIV-1 RNA were assayed in six replicates, whereas the reference genes TBP and IPO8 were assayed in duplicates. Droplet generation was done according to manufacturer's instructions using a QX100 droplet generator. The PCR reaction was carried out on a Bio-Rad CFX96 Thermal Cycler. Reading of droplets was by the QX100 droplet reader (Bio-Rad, USA). Data were analysed using QuantaSoftTM software (Bio-Rad, USA).

2.16. RNAScope/immunofluorescence (IF) multiplex

RNAScope/IF multiplex assays were performed to quantify the number of follicular dendritic cell-associated virions and HIV RNA positive cells. RNAScope/IF multiplex was performed on formalin-fixed paraffin-embedded (FFPE) 5 μm serial in essence as previously described [38] with some modifications. Sections were deparaffinized and rehydrated RNAScope/IF multiplex HIER was performed in boiling ACD target retrieval buffer for 15 min. Sections were deparaffinized and rehydrated and HIER was performed in boiling ACD target retrieval buffer for 15 min. Sections were treated with ACD Protease III (1:10 dilution in PBS) for 20 min at 40 °C, followed by ACD H_2O_2 treatment for 10 min at RT. Between steps, the sections were rinsed twice in dH_2O.

Target probes (HIV-1 Clade B # 41611, For ID117 HIV Clade C #429841, ACD) were incubated at 40 °C for 2 h and the signal was amplified according to ACD RNAScope2·5 HD BROWN kit protocol, with the exception that we utilized 0·5× wash buffer for all washing steps. Development of amplified RNA was performed with Tyramide signal amplification (TSA) reagent conjugated with Alexa Fluor™488 added in a 1:500 dilution for 10 min. Before incubating the anti-CD20 antibody overnight at 4 °C the sections were microwaved at power level 10 for 1 min followed by 15 min at power level 2, cooled for 10 min, washed twice with dH_2O and washed once with 0·1% TBS-Tween20. Anti-CD20 antibody stain was visualized using a Polink-2 Mouse polymer kit conjugated with Horseradish Peroxidase (GBI-labs) and TSA reagent conjugated with Alexa Fluor™594. Finally, CD35 was detected by incubating primary anti-CD35 antibody overnight at 4 °C followed by secondary anti-rabbit antibody conjugated with Alexa Fluor™647. DNA was visualized with DAPI (Invitrogen) 1:25,000 for 10 min. To prevent autofluorescence, sections were incubated with filtered Sudan Black (diluted 10:1 in 10xTBS) for 20 min, washed and mounted with Prolong Gold anti-fade mounting media. Sections were imaged and stitched using a Keyence BZ-X710 at 40× (Nikon Plan Apo; NA 0·60) and stitched using Keyence software.

2.17. Biostatistical analyses

Two-tailed Wilcoxon signed-rank tests were utilized to analyse changes from baseline, Spearman rank tests were used when detecting data correlations. The statistical comparisons and graphs were generated using GraphPad 7 and no outliers were censored. These are biological observations from the same lymph node materials. Therefore, the alpha was set to 0.05 without adjustments for the 121 statistical tests performed herein (97 Wilcoxon signed-rank tests +24 Spearman rank tests – excluding RNA sequencing analyses), according to the recommendation by Rothman [39]. Corrections for multiple comparisons were made during analyses of the RNA sequencing dataset as described above. Interpretations of the Spearman rank outcomes are based upon the approach published by Hinkle, Wiersma, & Jurs [40]. For r values between 0.90 and 1.00 (−0.90 and − 1.00), the interpretation was: very high positive (negative) correlation. For r values between 0.70 and 0.90 (−0.70 and − 0.90), the interpretation was: high positive (negative) correlation. For r values between 0.50 and 0.70 (−0.50 and − 0.70), the interpretation was: moderate positive (negative) correlation.

3. Results

3.1. Lymph nodes exhibited a potent interferon response following MGN1703 therapy

This was a predefined sub-study, which investigated the impact of 24 weeks MGN1703 treatment on lymph node biology. We included HIV-1 infected participants from a phase 1b/2a clinical study wherein they received MGN1703 (s.c., 60 mg 2× weekly for 24 weeks) concurrent with combination antiretroviral therapy (cART). The primary purpose of the trial was to pursue a potential role for TLR9 agonism in the context of HIV cure research and primary study outcomes have been reported previously [8]. Eight study participants (Table S4) volunteered for participation in the lymph node sub-study. Of these, seven participants completed the sub-study and provided inguinal lymph nodes for analyses at both baseline and during the last week of dosing (Week 24; Fig. 1a). Adverse events related to lymph node excisions were graded in accordance with the Common Terminology Criteria for Adverse Events (CTCAE) version 4.0 (Table S5).

Hallmarks of TLR9-agonist treatment are activation of pDCs, NK cells and T cells [6–8,41,42]. Therefore, we examined lymph node and peripheral blood mononuclear cells (LNMCs and PBMCs, respectively) of study participants at baseline and at 24 weeks of treatment for evidence of MGN1703-mediated immune cell activation. With respect to LNMC, we detected elevated expression ($p = 0·063$) of the activation markers CD86 and CD40 on pDCs (Figs. 1b-c and S1a) and a significant increase ($p = 0·031$) in the proportion of CD69-expressing LNMC NK cells during MGN1703 dosing (Figs. 1d and S1b). Within the lymph node T cell compartment, the greatest impact of MGN1703 dosing was observed in the context of the activation status of CD8+ T effector memory cells (HLA-DR+/CD38+; $p = 0·016$) (Figs. 1e and S1c-e). These LNMCs data are consistent with PBMC data from this study cohort [8].

Another hallmark of TLR9-agonist stimulation is activation of interferon response pathways [4,41]. To examine whether these and related pathways were affected in lymph nodes after 24 weeks of MGN1703 therapy, we performed longitudinal global transcriptomic analyses using RNASeq on LNMC from baseline and 24 weeks post therapy. The volcano plot in Fig. 1f and the Ingenuity Pathway Analyses in Table S6 illustrate the robust activation of gene expression related to both interferon as well as TLR signalling that we observed. Among the transcriptomic changes highlighted in Fig. 1f is the increased expression of interferon stimulated gene 15 (ISG15) in LNMC following MGN1703 treatment. Protein level confirmation of the RNASeq findings was demonstrated by quantitative immunohistochemistry on sections of lymph node tissues from this study cohort. Here, we found that ISG15 expression increased significantly in the lymph node cortex (Fig. 1g-h). Overall, the flow cytometry and RNASeq data together with the quantitative IHC findings reveal that 24 weeks of MGN1703 dosing resulted in a robust interferon response in the lymph nodes of the treated individuals.

3.2. MGN1703 induced B cell differentiation

B cell differentiation is a multi-stage process whereby B cells at distinct stages can be distinguished by their cell surface phenotype [43–45]. In the lymph node, B cell differentiation stages include transitional, naïve/mature, marginal zone, follicular, germinal center, switched memory and plasma blasts (gating strategy in Fig. S2a) [45]. These populations, with the exception of germinal center B cells, can also be found in peripheral blood (gating strategy in Fig. S2b) [44]. We examined LNMC (baseline and week 24) and PBMC (baseline, week 12 and week 24) by flow cytometry and found that MGN1703 dosing promotes B cell differentiation evidenced by increases in LNMC follicular and germinal center B cells as well as increases in both the proportion of LNMC and PBMC plasma blasts (Figs. 2a and S2c). Furthermore, when analysing the changes in the median size of LMNC and PBMC plasma blasts we found a significant increase in LMNC plasma blasts ($p = 0·047$), whereas PBMC plasma blast size were decreased after 12 weeks ($p = 0·034$) and unchanged after 24 weeks ($p = 0·30$). Also, we noted that there was an association between LNMC B cell maturation from germinal center B cells to plasma blasts ($p < 0·0001$; Fig. S2d). In addition, we analysed the levels of lymph node CD21low/CD38low activated B cells, as well as immature B cells; both were unchanged with treatment. These flow cytometry data are consistent with RNASeq data obtained from LNMCs and analysed according to the CIBERSORT algorithm [26]. Specifically, the algorithm identified a gene expression profile consistent with significantly more plasma cells in the LNMC pool following MGN1703 dosing (Fig. 2b). Knowing that MGN1703 dosing was inducing B cells to differentiate towards plasma cells led us to examine the lymph node architecture for the presence of primary and secondary follicles. When we examined the lymph nodes at baseline versus 24 weeks post treatment, we found that the number of primary follicles was trending downwards while the number of secondary follicles was trending upwards (Fig. 2c-d). These data may indicate that TLR9 agonism contributes to the restoration of lymph node architecture and function. Taken together, these data reveal that B cell differentiation, maturation and functional potential are augmented in the presence of MGN1703 in vivo.

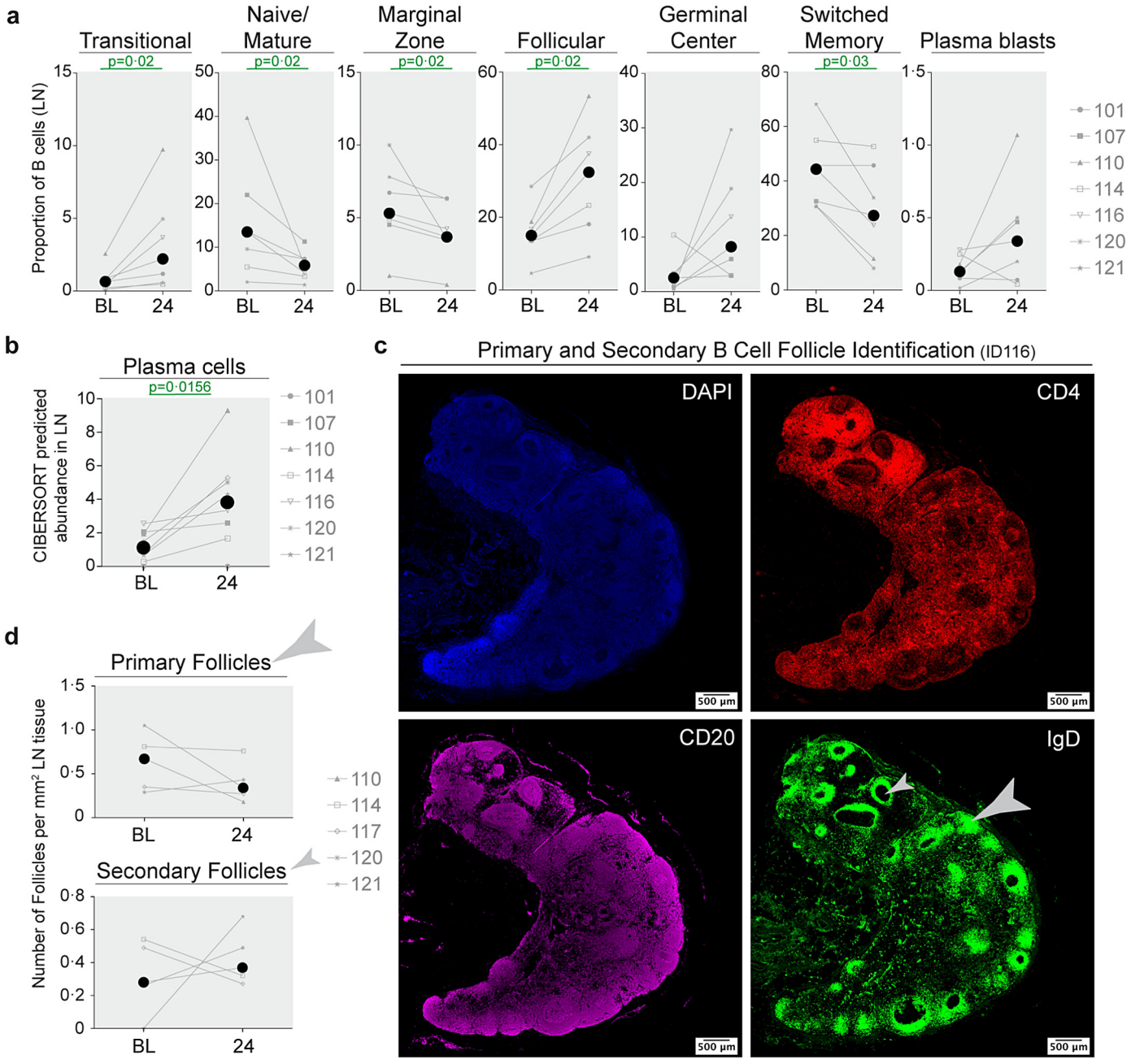

Fig. 2. MGN1703 induces peripheral blood and lymph node B cell differentiation. (a) The proportions of lymph node B cell lineages were impacted by MGN1703 treatment. Flow cytometry gating for B cell lineages as well as additional PB B cell lineage results are presented in Fig. S2. (b) Plot shows the abundance of lymph node plasma cells predicted by CIBERSORT [26]. (c-d) Representative images of immunofluorescent multiplex lymph node analyses (c) and quantitation of primary (large arrows) and secondary (small arrows) B cell follicles (d). DAPI: nuclei, CD4: CD4+ T cells, CD20: B cells, and IgD: naïve B cells. B cell follicles were defined as secondary when IgD was excluded from germinal centers. Statistics: Wilcoxon matched-pairs signed-rank test (a-b, d). Axis time notations: baseline (BL) and 24 weeks (24). The n value for each analysis is defined via individual participant data points, which are graphed with grey symbols/lines and defined in adjacent legends or individually labelled in correlation plots. Black circles represent median points.

3.3. MGN1703 increased proportions of lymph node T follicular helper (Tfh) cells

The changes in the B cell compartment that we observed following MGN1703 dosing led us to also examine the T cell compartment with a focus on Tfh cells. The primary function of Tfh cells is to provide "help" in the positive selection of high affinity B cells as the B cells experience antigenic stimulation towards proliferation and differentiation into plasma cells [12]. Using quantitative immunohistochemistry, we showed that the ratio of CD4+ T cell found within B cell follicles versus CD4+ T cells in the T cell zones of the lymph node tended to increase in all participants analysed ($p = 0{\cdot}063$; Fig. 3a-b). This finding was consistent with our flow cytometry observation as well as our RNASeq/CIBERSORT findings that revealed higher proportions of Tfh cells within the total lymph node mononuclear cell compartment with MGN1703 treatment (Fig. 3c-d). These changes in lymph node Tfh levels were not associated with changes of this cell type in peripheral blood as seen in Fig. S3. However, we found that an increase in PBMC Tfh cells was moderately negatively correlated with an increase in PBMC plasma blasts ($p = 0{\cdot}049$; $r = -0.59$) indicating that the maturation of B cells into plasma blasts may be T cell dependent (Fig. S3). Comparing the changes in lymph node Tfh cells with plasma blasts ($p = 0{\cdot}058$; Fig. 3e) and lymph node Tfh cells with germinal center B cells ($p = 0{\cdot}058$; $r = 0{\cdot}8286$) we observed an analogous outcome. In

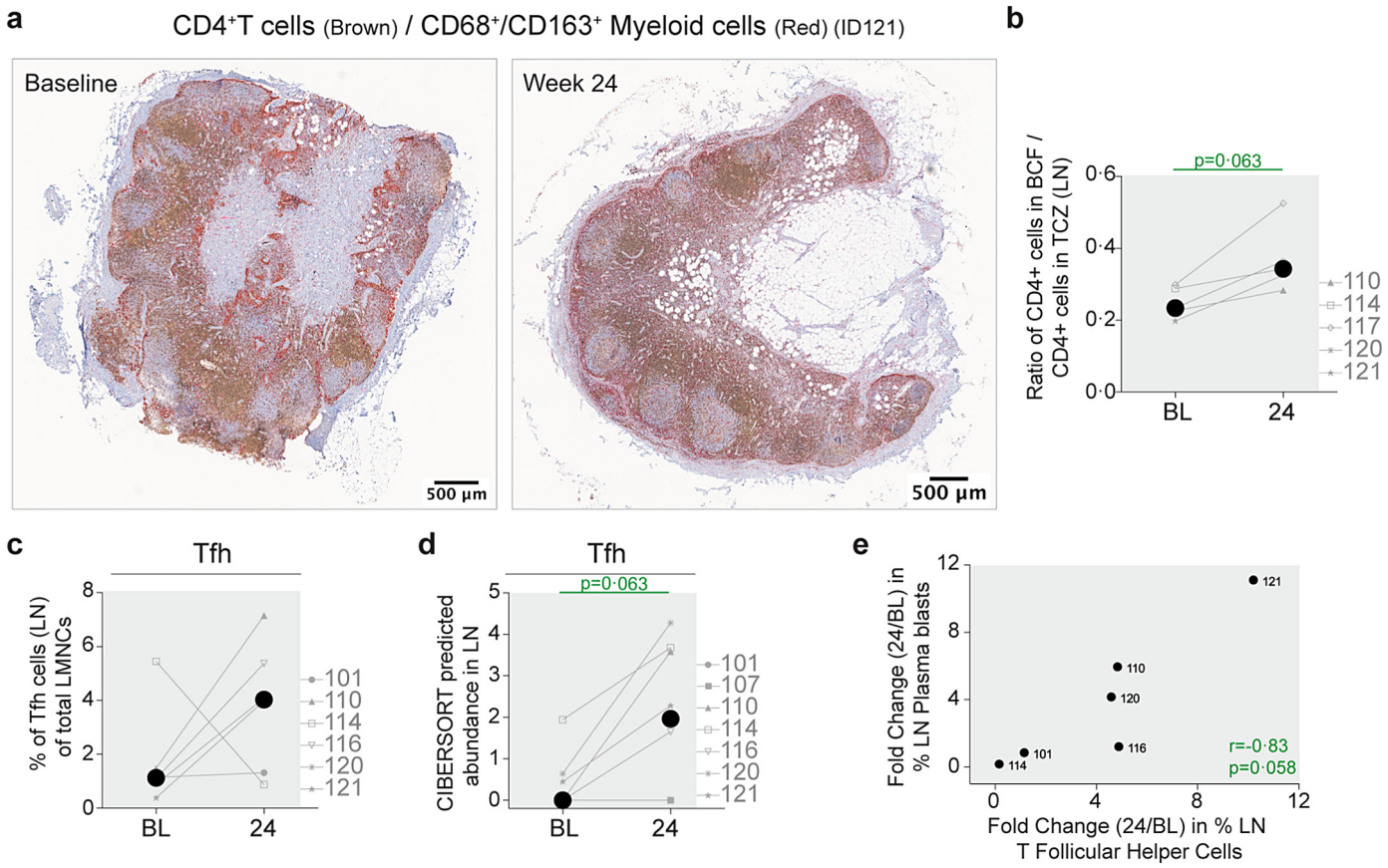

Fig. 3. MGN1703-induced B cell differentiation is associated with increased proportions of T follicular helper cells in peripheral blood and lymph nodes. (a) Example baseline and on treatment (week 24) immunohistochemistry stains for CD4 are shown. This stain was performed prior to quantitation of the frequency of CD4+ T cell profiles in B cell follicles (BCF) and T cell zones (TZC). Co-staining with the myeloid markers CD68 and CD163 was incorporated to facilitate differentiation between CD4+ T cells and CD4+ macrophages. (b) The frequency of CD4+ T cells in BCFs and TCZs was quantified and the ratios of CD4+ T cells in the BCFs and TZC are presented. (c) Proportions of lymph node Tfh cells (CD3 + CD4 + CD45RA–CXCR5 + PD–1+) within the total lymph node mononuclear cell compartment are presented. Flow cytometry gating for Tfh cells is presented in Fig. S3a. Proportions of peripheral blood Tfh cells are presented in Fig. S3b (d) Plot shows the abundance of lymph node Tfh cells estimated using CIBERSORT [26]. (e) Plot shows a positive association between changes in proportions of plasma blasts and Tfh cells in lymph nodes. Plot showing a positive association between changes in proportions of plasma blasts and Tfh cells in peripheral blood is presented in Fig. S3c. Statistics: Wilcoxon matched-pairs signed-rank test (b-d) or Spearman rank test (e). Axis time notations: baseline (BL) and 24 weeks (24). The n value for each analysis is defined via individual participant data points, which are graphed with grey symbols/lines and defined in adjacent legends or individually labelled in correlation plots. Black circles represent median points.

summary, MGN1703 dosing led to increased proportions of Tfh cells and this effect was particularly notable in lymph node, which is the anatomical location for Tfh function.

3.4. MGN1703 increased IgG production and AID expression

When we quantitated plasma levels of total IgG as well as IgG subclasses, we observed significantly elevated levels of total IgG, IgG1, IgG2, and IgG3 at week 12 of treatment versus baseline (Fig. 4a). In line with the results shown in Fig. 3e and Fig. S3c we also observed a very high correlation between the increase in total plasma IgG at week 12 and the increase in LNMC Tfh cells at week 24 ($p = 0{\cdot}017$, $r = 0.94$; Fig. 4b) supporting the idea that TLR9 agonist enhancement of B cells involves T cell help. The observed changes in IgG subtypes and the fact that B cell differentiation typically is associated with antibody class switching and affinity maturation [46] led us to look into the expression of the activation-induced cytidine deaminase (AID) gene, a key regulator of B cell diversification and somatic hypermutation. LNMC RNASeq analyses at week 24 showed a 5·65-fold increase in expression compared to baseline (Fig. 4c) indicating that the potential for somatic hypermutation is induced by MGN1703 treatment.

We previously showed that MGN1703 might induce latent HIV expression in some individuals [7]. Therefore, we hypothesized that despite ongoing cART during MGN1703 dosing; there could be low-level expression of HIV antigens towards which the elevated antibody response could be directed. We tested both aspects of this hypothesis including changes in viral RNA levels as well as antibody neutralization capacity. Regarding viral nucleic acids: Among the seven individuals included in this study, we did not observe cohort-wide changes in LNMC-associated HIV DNA or RNA levels (Fig. S4a-b). Furthermore, when we performed fluorescence in situ hybridization assays (i.e. RNAScope) on sections of lymph node tissue to detect follicular dendritic cell-bound virions and viral RNA positive cells, we found a paucity of HIV RNA within lymph nodes (Fig. S5). Specifically, no follicular dendritic cell-associated virions were observed within the 34·6 mm^2 of B cell follicles that were analysed. This area of B cell follicles inspected is the aggregate area from the total of fifty-six 5 µm sections assessed. In 17·2 mm^2 of T cell zones that were visually inspected, we only found four HIV RNA positive cells. Thus, we did not find evidence of MGN1703-induced latency reactivation in lymph nodes at week 24. Regarding antibody neutralization capacity: We found that the MGN1703-mediated upregulation of six immunoglobulin light chain genes and one Ig heavy chain variable gene were associated with MGN1703-induced reduction of HIV DNA levels in LNMCs (Fig. S4c). These data combined with our finding that changes in plasma IgG levels were highest at week 12 (Fig. 4a), led us to assess plasma antibodies' anti-HIV capacity using a standard HIV neutralization assay developed for identifying broadly HIV neutralizing antibodies [36]. As the majority of Danish HIV-infected individuals are infected with subtype B virus, we stratified

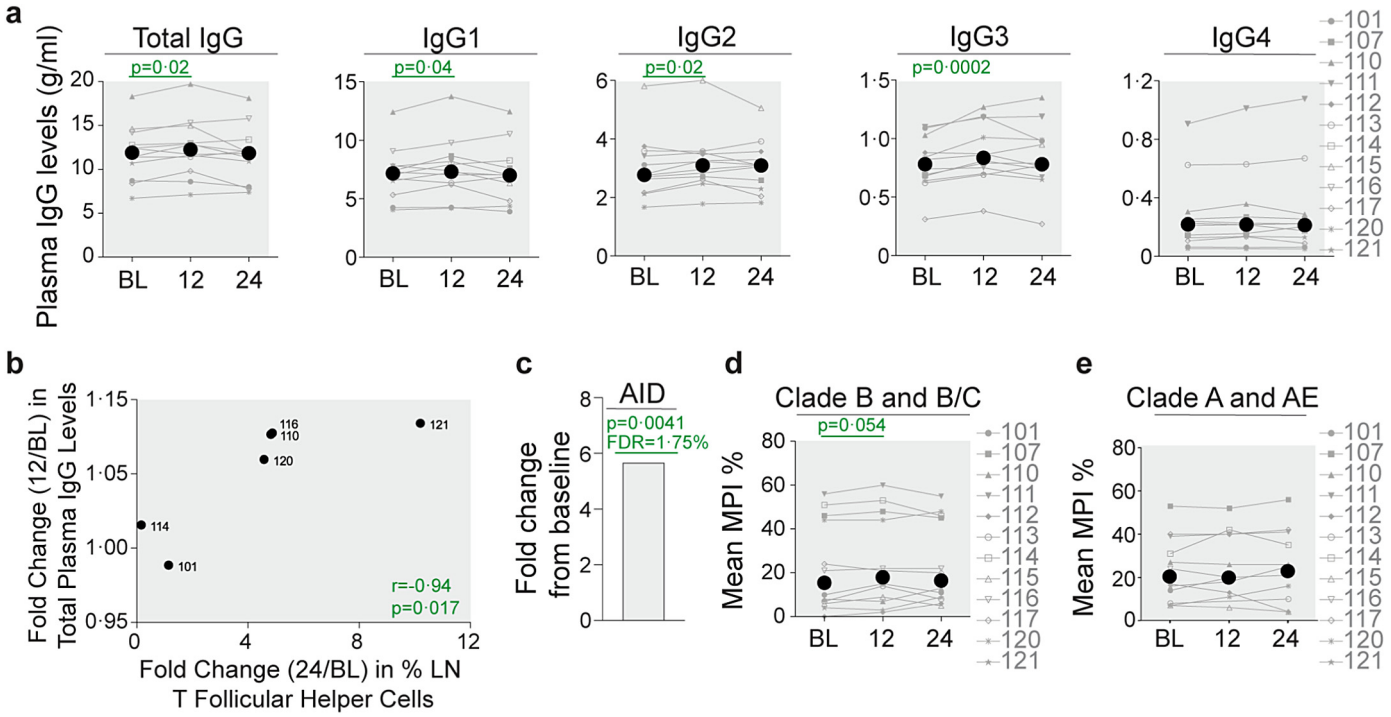

Fig. 4. MGN1703 induces plasma IgG secretion that specifically neutralize HIV clade B and C. (a) Plasma IgG and IgG subtype levels are shown. (b) Plot shows a positive association between the changes in plasma IgG and the changes in lymph node Tfh cells. (c) Graph shows the fold change of Activation-Induced cytidine Deaminase (AID) expression from baseline to on MGN1703 treatment at 24 weeks (d-e) Neutralization outcomes against Clade B and B/C (d) and Clade A and AE (e) envelopes are depicted. MPI = maximum percent inhibition. Statistics: Wilcoxon matched-pairs signed-rank tests for on treatment timepoints vs. baseline (a; d-e) or Spearman rank test (b). Axis time notations: baseline (BL), 8 weeks (8), 12 weeks (12), and 24 weeks (24). The n value for each analysis is defined via individual participant data points, which are graphed with grey symbols/lines and defined in adjacent legends or individually labelled in correlation plots. Black circles represent median points.

the neutralizing capacity data into B and BC clades or A and AE clades. We identified a trend towards an elevated ($p = 0{\cdot}054$) clade B/BC neutralizing capacity at week 12 when the increased total levels of IgG in plasma were also observed (Fig. 4d), whereas there was no change in the ability of the patient IgG to neutralize clade A and AE envelopes (Fig. 4e). Together these data indicate that MGN1703 dosing induced increases in plasma IgG secretion with potential affinity maturation of these antibodies towards HIV clade B/BC specificity.

3.5. MGN1703 modulated antibody glycosylation patterns

We examined the glycosylation patterns on peripheral blood- as well as lymph node-derived antibodies. We observed that multiple major glycosylation patterns (e.g. sialylated and galactosylated) were modulated by TLR9 agonist treatment in both compartments (Figs. 5a and S6). The glycosylation changes on plasma antibodies were observed at both week 12 and week 24. We next examined whether the changes in plasma antibody glycosylation patterns were associated with changes in the size of the HIV reservoir. We identified strong associations between specific glycosylation patterns and reductions in the HIV reservoir measurements (Fig. 5b-d). We noted that decreases in grouped mono-galactosylated plasma antibodies were highly negatively correlated with increased levels of HIV RNA in circulating CD4+ T cells ($p = 0{\cdot}018$, $r = -0.77$; Fig. 5b). We also observed that increases in grouped sialylated plasma antibodies were highly negatively correlated with reduced levels of HIV DNA in CD4+ T cells ($p = 0{\cdot}018$, $r = -0.71$; Fig. 5c). Similarly, we found that increases in levels of A2G2S1 glycan motif on plasma antibodies were moderately negatively correlated with reduced levels of HIV DNA in circulating CD4+ T cells ($p = 0{\cdot}031$, $r = -0.66$; Fig. 5d). In conclusion, we found that MGN1703 significantly altered antibody glycosylation patterns and key glycosylation changes can be linked with reduction in HIV reservoirs.

4. Discussion

In this study, we longitudinally analysed the impact of MGN1703 on mononuclear cells within inguinal lymph nodes and peripheral blood of HIV infected individuals. We found that MGN1703 activated pDCs, NK cells, and T cell as well as induced a robust interferon response in lymph nodes. Furthermore, we found that MGN1703 dosing increased B cell differentiation and secondary B cell follicle formation. Changes in B cell population dynamics were accompanied by increased IgG production and changes in antibody glycosylation patterns. The latter was associated with reductions in the levels of HIV persisting within the lymph nodes during cART.

In the current study, we examined inguinal lymph nodes, as representative secondary lymphoid tissues, for evidence of tissue penetration and sustained activity of MGN1703 in these anatomical sites. We did this because data detailing the effects of in vivo TLR9 agonism within human tissues are very limited. Lymph node effects of TLR9 agonism exists in the context of cross-sectional studies, which probed the effects of CPG ODNs on dendritic cells present in sentinel lymph nodes from early stage melanoma patients [47–49]. Beyond lymph nodes, we have published a longitudinal study showing that MGN1703 induced a type I, but not a type II, interferon response in a mucosal site – namely the sigmoid colon of HIV infected persons [6]. In contrast to many of our mucosal tissue findings [6], the activation of T cells that we observed here in the lymph nodes was similar to our peripheral blood findings at the same time points [8]. We also observed similar levels of NK cell and pDC activation when comparing lymph node and peripheral blood results. Thus, TLR9 agonism-induced outcomes in blood and lymph node resemble each other more so than blood and sigmoid colon outcomes. There are major distinctions in the physiological roles of mucosal tissues versus secondary lymphoid tissues that likely explain the differences observed. Specifically, the lymph nodes are anatomical sites for the generation of adaptive immune responses whereas the immune responses

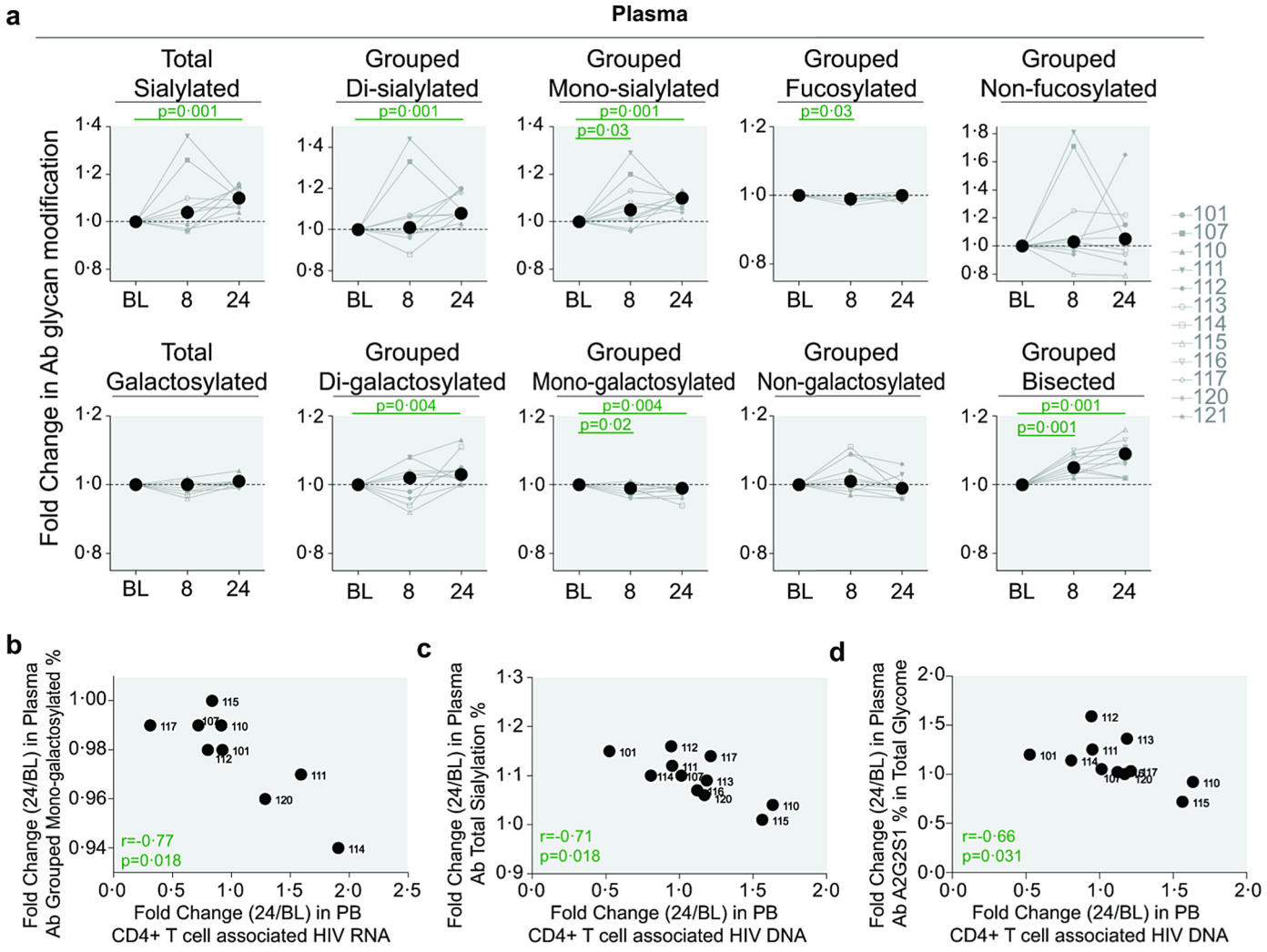

Fig. 5. MGN1703 changes plasma antibody glycosylation patterns. (a) Immunoglobulin glycosylation profiles were assessed in plasma. Immunoglobulin glycosylation profiles assessed in lymph node wash are shown in Fig. S5. (b-d) Plots show negative associations between key plasma antibody glycosylation parameters and changes in PB CD4+ T cell-associated HIV-1 RNA/DNA. Total lymph node mononuclear cell-associated HIV-1 RNA/DNA is presented in Fig. S4a-b. Statistics: Wilcoxon matched-pairs signed-rank tests for on treatment timepoints vs. baseline (a) or Spearman rank test (20 total performed) (b-d). Axis time notations: baseline (BL), 8 weeks (8), and 24 weeks (24). The n value for each analysis is defined via individual participant data points, which are graphed with grey symbols/lines and defined in adjacent legends or individually labelled in correlation plots. Black circles represent median points.

in the intestines are tightly regulated to prevent hyper-inflammation directed towards the constantly present stimulatory milieu at this anatomical site.

We present evidence of TLR9 agonist induced effects on B cell differentiation, maturation and function in both peripheral blood and lymph nodes. Consistent with follicular B cells aggregating in lymph nodes and differentiating into germinal center B cells [12], we observed increases in follicular B cell population in lymph nodes simultaneous to this population becoming proportionally smaller in the peripheral blood. Furthermore, this change in lymph node follicular B cells occurred as the germinal center B cell population, which increased in 5 of 7 lymph node pairs evaluated. Moreover, we observed architectural differences during MGN1703 treatment with respect to increased numbers of secondary B cell follicles – the primary anatomical location for antibody affinity maturation. The changes in B cell populations and lymph node architecture were accompanied by increases in plasma IgG levels at week 12. As these changes are subtle, the biological relevance of the changes is not proven here. However, it is important to note that these data align line with previous data showing increase in IgG production following ex vivo MGN1703-stimulation of PBMCs [50]. The 12 week time point is in accordance with the time point where we observed a modest increase in HIV neutralization capacity by plasma antibodies. While it is well established that B cell population abnormalities and dysfunctions result from HIV infection [51–54], our LNMC RNASeq data showed a 5·65-fold increase in expression of activation-induced cytidine deaminase (AID) at week 24. AID enzymatic activity is critical for both antibody class switching as well as somatic hypermutation leading to antibody affinity maturation [55]. Thus, our data suggests that MGN1703 treatment changes B cell differentiation in HIV-infected individuals. Since these changes were associated with increases in Tfh cell proportions and increased AID expression, it is likely that the changes in antibody production were T-dependent in nature.

Beyond their well described fundamental roles in initiating and maintaining adaptive immune responses, lymph nodes are of particular interest in HIV infection. First, lymph node architecture of distinctly defined B cell follicles and T cells zones is disrupted during untreated infection by fibrosis and this damage is not fully reversed by long-term standard-of-care treatment (cART) [56–59]. Thus, the observed trends towards secondary B cell follicle formation suggest that repeated TLR9 agonism can further reverse HIV-induced lymph node damage that accumulates prior to cART administration. A second reason that lymph nodes are of particular interest in HIV infected persons, is that lymph nodes harbor persistent HIV reservoirs during cART and these viral reservoirs represent the greatest barrier to a cure for HIV [60–63]. Despite the recognized importance of lymph nodes in HIV disease, there is limited longitudinal lymph node data to provide insights into the stability

of the persistent HIV reservoir in lymph nodes during cART [64]. Recently published data from some of these same lymph nodes show that the latent viruses found in circulation overlap genetically with those found in lymph nodes and that the overall frequency of HIV-1 proviruses in blood and lymph node CD4+ T cells was the same [65]. Our current study of these lymph nodes provides much needed insight into the longitudinal stability of the HIV reservoir in lymph nodes, which is of paramount importance in the realization of an HIV cure. One of the mechanisms of HIV persistence in lymph nodes is via virions being trapped and retained on follicular dendritic cells as we and others have shown in HIV as well as SIV infection [38,60,64,66,67]. Here, we could not identify follicular dendritic cell-associated virions in any lymph node sample analysed – including baseline samples. As was true for locating follicular dendritic cell-associated virions, we found HIV RNA producing cells to be exceedingly rare in the lymph nodes of our study population, even at baseline. Our observations of rare HIV RNA-associated cells in lymph nodes could be explained, at least in part, by the fact that participants in this lymph node study had been taking cART for a median of 6.3 years which is well beyond the 30 months of triple antiretroviral therapy previously estimated to be required for elimination of viral RNA in secondary lymphoid tissues, specifically tonsils [68].

Glycans are highly diverse and complex carbohydrate structures composed of branched monosaccharide chains [69]. Glycans are added to many biological molecules (including proteins and lipids) via glycosylation. We detected an increase in plasma IgGs after 12 weeks and these plasma antibodies, as well as lymph node-derived antibodies, exhibited MGN1703-dosing associated changes in glycosylation. Previous publications showed that even subtle glycan modulations can lead to significant differences in antibody activities, and that minor glycan species can play a significant role in antibody effector function [70,71]. Interestingly, the significant changes in glycosylation on peripheral blood antibodies were generally in the opposite direction from the changes observed in lymph nodes. For example, the increases in grouped di-sialylated motifs on plasma antibodies at week 24 contrasted with the downward trend for this parameter observed on lymph node antibodies. These differences could reflect anatomical sequestration of antibodies with specific glycosylation patterns based upon a given antibody's likely effector function [e.g. antibody dependent cellular cytotoxicity (ADCC), antibody dependent cellular phagocytosis (ADCP), and antibody dependent complement deposition (ADCD)] [72–76]. When we focused our association analyses in the peripheral blood, we found that increases in plasma antibodies bound to glycan motifs that included galactose and sialic acid molecules were negatively correlated with reductions in PBMC-associated HIV DNA and RNA levels. This is consistent with our prior work documenting that higher levels of multiple glycosylation motifs, particularly those that non-fucosylated galactosylated, are associated with lower levels of cell-associated HIV DNA and RNA in vivo [77]. Our current data linking glycosylation with changes in HIV reservoir measurements highlight the potential beneficial effects of MGN1703-mediated modulation of antibody glycosylation patterns. These data also substantiate previous work showing the importance of these glycosylation motifs in clearing persistent HIV, potentially via non-neutralizing Fc-mediated effector functions of antibodies.

5. Conclusions

In this study, we present 24-week longitudinal analyses of human lymph node immunology and HIV virology as we determined the impact of TLR9 agonism in these important secondary lymphoid tissues. We found that the impact of TLR9 agonism on lymph node lymphocyte activation and B cell differentiation closely resembled outcomes in peripheral blood at match time points. We also report changes in B cell population dynamics, increase in plasma IgG levels, increase in AID, and changes in antibody glycosylation, which is known to have functional implications. Finally, we show that specific antibody glycosylation patterns associated with reductions in HIV reservoir levels. TLR9 agonism is a component of multiple planned and ongoing HIV cure related clinical interventions (e.g. NCT03837756). In this context, these lymph node data are of exceptional value for future HIV cure related clinical trials to guide their planning and interpretation. The lymph node data provided here will also be of immediate value in the context of oncological indications where they will contribute to the interpretation of incoming phase 3 trial data and the planning of future studies.

Acknowledgements

We thank the participants for their generous contribution to the study as well as Lene Svinth Jønke and Helena M. Andersen for laboratory assistance.

Funding sources

Fulbright Visiting Scholar Award to MHS, Augustinus Foundation (17–3250; MHS), Julie von Müllers Foundation award to MHS, Aarhus University Research Foundation (AUFF-E-2016-FLS-8-9; PWD); Danish Council for Independent Research (DFF-6120-00017 and DFF-7025-00022; PWD), and the Novo Nordisk Foundation (NNF17OC0028462; MT). PS and FK were supported by the German Center for Infection Research (DZIF) and the European Research Council (ERC-StG639961). Mologen AG provided study drug free of charge. The funders had no role in study design, data collection, data analyses, interpretation, or writing of the report.

Declarations of interest

BW reports personal fees and other from MOLOGEN AG, during the conduct of the study. BW is listed as inventor of an issued patent family, owned by MOLOGEN AG, protecting the TLR9 agonist (dSLIM®, MGN1703), used in the trial; INN Lefitolimod.

JDE reports personal fees from Advanced Cell Diagnostics, outside the submitted work.

MS is an employee of Mologen AG. MS, MT and OSS have a patent Schroff M, Schmidt M, Kapp K, Zurlo A, Tolstrup M, Offersen R, Søgaard OS: MEANS FOR THE TREATMENT OF HIV Pub. No WO/2017/050806 issued to Mologen AG.

Author contributions

Concept development: PWD, MHS, OSS, MT, LØ, and LV. Clinical study and collection of patient material: LV, PWD, TD, PA, and MBH. Performed data collection: MHS, M-LK, LV, KK, LBG, KB-S, CNC, MN, KZ, FHR, RO, PS, HD, and AK. Performed data analyses and interpretation of the results: MHS, M-LK, LV, KK, LBG, KB-S, CNC, MN, MS, BW, KZ, FHR, RO, PS, FK, HD, AK, JRN, JDE, MA-M, MT, OSS, and PWD. First draft of the manuscript: MHS and PWD. Critically revising the manuscript for important intellectual content: all authors.

Data and materials availability

The RNA-seq data was deposited to GEO (https://www.ncbi.nlm.nih.gov/geo/) under accession number GSE130307.

Appendix A. Supplementary data

Supplementary data to this article can be found online at https://doi.org/10.1016/j.ebiom.2019.07.005.

References

[1] O'Neill LA, Golenbock D, Bowie AG. The history of toll-like receptors - redefining innate immunity. Nat Rev Immunol 2013;13(6):453–60.

[2] Kapp K, Kleuss C, Schroff M, Wittig B. Genuine immunomodulation with dSLIM. Mol Ther Nucleic Acids 2014;3:e170.
[3] Kawai T, Akira S. Toll-like receptors and their crosstalk with other innate receptors in infection and immunity. Immunity 2011;34(5):637–50.
[4] Wittig B, Schmidt M, Scheithauer W, Schmoll HJ. MGN1703, an immunomodulator and toll-like receptor 9 (TLR-9) agonist: from bench to bedside. Crit Rev Oncol Hematol 2015;94(1):31–44.
[5] Della Chiesa M, Romagnani C, Thiel A, Moretta L, Moretta A. Multidirectional interactions are bridging human NK cells with plasmacytoid and monocyte-derived dendritic cells during innate immune responses. Blood 2006;108(12):3851–8.
[6] Krarup AR, Abdel-Mohsen M, Schleimann MH, et al. The TLR9 agonist MGN1703 triggers a potent type I interferon response in the sigmoid colon. Mucosal Immunol 2017;11(2):449–61.
[7] Vibholm L, Schleimann MH, Hojen JF, et al. Short-course toll-like receptor 9 agonist treatment impacts innate immunity and plasma viremia in individuals with human immunodeficiency virus infection. Clin Infect Dis 2017;64(12):1686–95.
[8] Vibholm LK, Konrad CV, Schleimann MH, et al. Effects of 24 week toll-like receptor 9 agonist treatment in HIV-1+ individuals: a single-arm, phase 1B/2A trial. AIDS (London, England) Jul 1 2019;33(8):1315–25.
[9] Schmoll HJ, Wittig B, Arnold D, et al. Maintenance treatment with the immunomodulator MGN1703, a toll-like receptor 9 S(TLR9) agonist, in patients with metastatic colorectal carcinoma and disease control after chemotherapy: a randomised, double-blind, placebo-controlled trial. J Cancer Res Clin Oncol 2014;140(9):1615–24.
[10] Thomas M, Ponce-Aix S, Navarro A, et al. Immunotherapeutic maintenance treatment with toll-like receptor 9 agonist lefitolimod in patients with extensive-stage small-cell lung cancer: results from the exploratory, controlled, randomized, international phase II IMPULSE study. Ann Oncol 2018;29(10):2076–84.
[11] Weihrauch MR, Richly H, von Bergwelt-Baildon MS, et al. Phase I clinical study of the toll-like receptor 9 agonist MGN1703 in patients with metastatic solid tumours. Eur J Cancer 2015;51(2):146–56.
[12] Mesin L, Ersching J, Victora GD. Germinal Center B cell dynamics. Immunity 2016;45(3):471–82.
[13] Willard-Mack CL. Normal structure, function, and histology of lymph nodes. Toxicol Pathol 2006;34(5):409–24.
[14] Dorner M, Brandt S, Tinguely M, et al. Plasma cell toll-like receptor (TLR) expression differs from that of B cells, and plasma cell TLR triggering enhances immunoglobulin production. Immunology 2009;128(4):573–9.
[15] Bekeredjian-Ding I, Jego G. Toll-like receptors–sentries in the B-cell response. Immunology 2009;128(3):311–23.
[16] Jiang W, Lederman MM, Harding CV, Rodriguez B, Mohner RJ, Sieg SF. TLR9 stimulation drives naive B cells to proliferate and to attain enhanced antigen presenting function. Eur J Immunol 2007;37(8):2205–13.
[17] Krieg AM, Yi AK, Matson S, et al. CpG motifs in bacterial DNA trigger direct B-cell activation. Nature 1995;374(6522):546–9.
[18] Bernasconi NL, Onai N, Lanzavecchia A. A role for toll-like receptors in acquired immunity: up-regulation of TLR9 by BCR triggering in naive B cells and constitutive expression in memory B cells. Blood 2003;101(11):4500–4.
[19] Ozcan E, Rauter I, Garibyan L, Dillon SR, Geha RS. Toll-like receptor 9, transmembrane activator and calcium-modulating cyclophilin ligand interactor, and CD40 synergize in causing B-cell activation. J Allergy Clin Immunol 2011;128(3):601–9 [e1-4].
[20] Ruprecht CR, Lanzavecchia A. Toll-like receptor stimulation as a third signal required for activation of human naive B cells. Eur J Immunol 2006;36(4):810–6.
[21] Abu-Rish EY, Amrani Y, Browning MJ. Toll-like receptor 9 activation induces expression of membrane-bound B-cell activating factor (BAFF) on human B cells and leads to increased proliferation in response to both soluble and membrane-bound BAFF. Rheumatology (Oxford) 2013;52(7):1190–201.
[22] Simchoni N, Cunningham-Rundles C. TLR7- and TLR9-responsive human B cells share phenotypic and genetic characteristics. J Immunol 2015;194(7):3035–44.
[23] Langmead B, Salzberg SL. Fast gapped-read alignment with bowtie 2. Nat Methods 2012;9(4):357–9.
[24] Li B, Dewey CN. RSEM: accurate transcript quantification from RNA-Seq data with or without a reference genome. BMC Bioinform 2011;12:323.
[25] Love MI, Huber W, Anders S. Moderated estimation of fold change and dispersion for RNA-seq data with DESeq2. Genome Biol 2014;15(12):550.
[26] Newman AM, Liu CL, Green MR, et al. Robust enumeration of cell subsets from tissue expression profiles. Nat Methods 2015;12(5):453–7.
[27] Benjamini Y, Drai D, Elmer G, Kafkafi N, Golani I. Controlling the false discovery rate in behavior genetics research. Behav Brain Res 2001;125(1–2):279–84.
[28] Deleage C, Schuetz A, Alvord WG, et al. Impact of early cART in the gut during acute HIV infection. JCI Insight 2016;1(10).
[29] Christensen AB, Dige A, Vad-Nielsen J, et al. Administration of Panobinostat is Associated with increased IL-17A mRNA in the intestinal epithelium of HIV-1 patients. Mediators Inflamm 2015;2015:120605.
[30] Sarzotti-Kelsoe M, Bailer RT, Turk E, et al. Optimization and validation of the TZM-bl assay for standardized assessments of neutralizing antibodies against HIV-1. J Immunol Methods 2014;409:131–46.
[31] Derdeyn CA, Decker JM, Sfakianos JN, et al. Sensitivity of human immunodeficiency virus type 1 to the fusion inhibitor T-20 is modulated by coreceptor specificity defined by the V3 loop of gp120. J Virol 2000;74(18):8358–67.
[32] Platt EJ, Bilska M, Kozak SL, Kabat D, Montefiori DC. Evidence that ecotropic murine leukemia virus contamination in TZM-bl cells does not affect the outcome of neutralizing antibody assays with human immunodeficiency virus type 1. J Virol 2009;83(16):8289–92.
[33] Platt EJ, Wehrly K, Kuhmann SE, Chesebro B, Kabat D. Effects of CCR5 and CD4 cell surface concentrations on infections by macrophagetropic isolates of human immunodeficiency virus type 1. J Virol 1998;72(4):2855–64.
[34] Takeuchi Y, McClure MO, Pizzato M. Identification of gammaretroviruses constitutively released from cell lines used for human immunodeficiency virus research. J Virol 2008;82(24):12585–8.
[35] Wei X, Decker JM, Liu H, et al. Emergence of resistant human immunodeficiency virus type 1 in patients receiving fusion inhibitor (T-20) monotherapy. Antimicrob Agents Chemother 2002;46(6):1896–905.
[36] deCamp A, Hraber P, Bailer RT, et al. Global panel of HIV-1 Env reference strains for standardized assessments of vaccine-elicited neutralizing antibodies. J Virol 2014;88(5):2489–507.
[37] Leth S, Nymann R, Jørgensen S, et al. HIV-1 transcriptional activity during frequent longitudinal sampling in aviremic patients on ART. AIDS (London, England) 2016;30(5):713–21.
[38] Deleage C, Wietgrefe SW, Del Prete G, et al. Defining HIV and SIV reservoirs in lymphoid tissues. Pathog Immunol 2016;1(1):68–106.
[39] Rothman KJ. No adjustments are needed for multiple comparisons. Epidimiology 1990;1(1):43–6.
[40] Hinkle DE, Wiersma WSJ. Applied statistics for the behavioural sciences. . 5th ed.Boston, USA: Houghton Mifflin; 2002.
[41] Krieg AM. Therapeutic potential of toll-like receptor 9 activation. Nat Rev Drug Discov 2006;5(6):471–84.
[42] Offersen R, Nissen SK, Rasmussen T, et al. A novel toll-like receptor-9 agonist, MGN1703, enhances HIV-1 transcription and NK cell-mediated inhibition of HIV-1 infected autologous CD4+ T-cells. J Virol 2016;90(9):4441–53.
[43] Martinez-Torres F, Nochi T, Wahl A, Garcia JV, Denton PW. Hypogammaglobulinemia in BLT humanized mice—an animal model of primary antibody deficiency. PLoS One 2014;9(10):e108663.
[44] Thorarinsdottir K, Camponeschi A, Cavallini N, et al. CD21(−/low) B cells in human blood are memory cells. Clin Exp Immunol 2016;185(2):252–62.
[45] Warnatz K, Schlesier M. Flowcytometric phenotyping of common variable immunodeficiency. Cytometry B 2008;74(5):261–71.
[46] Hoffman W, Lakkis FG, Chalasani G. B cells, antibodies, and more. Clin J Am Soc Nephrol 2016;11(1):137–54.
[47] Molenkamp BG, Sluijter BJ, van Leeuwen PA, et al. Local administration of PF-3512676 CpG-B instigates tumor-specific CD8+ T-cell reactivity in melanoma patients. Clin Cancer Res 2008;14(14):4532–42.
[48] Molenkamp BG, van Leeuwen PA, Meijer S, et al. Intradermal CpG-B activates both plasmacytoid and myeloid dendritic cells in the sentinel lymph node of melanoma patients. Clin Cancer Res 2007;13(10):2961–9.
[49] Sluijter BJ, van den Hout MF, Koster BD, et al. Arming the melanoma sentinel lymph node through local administration of CpG-B and GM-CSF: recruitment and activation of BDCA3/CD141(+) dendritic cells and enhanced cross-presentation. Cancer Immunol Res 2015;3(5):495–505.
[50] Schmidt M, Anton K, Nordhaus C, Junghans C, Wittig B, Worm M. Cytokine and Ig-production by CG-containing sequences with phosphorodiester backbone and dumbbell-shape. Allergy 2006;61(1):56–63.
[51] De Milito A, Nilsson A, Titanji K, et al. Mechanisms of hypergammaglobulinemia and impaired antigen-specific humoral immunity in HIV-1 infection. Blood 2004;103(6):2180–6.
[52] Kovacs JA, Lempicki RA, Sidorov IA, et al. Identification of dynamically distinct subpopulations of T lymphocytes that are differentially affected by HIV. J Exp Med 2001;194(12):1731–41.
[53] Moir S, Ho J, Malaspina A, et al. Evidence for HIV-associated B cell exhaustion in a dysfunctional memory B cell compartment in HIV-infected viremic individuals. J Exp Med 2008;205(8):1797–805.
[54] Moir S, Malaspina A, Ogwaro KM, et al. HIV-1 induces phenotypic and functional perturbations of B cells in chronically infected individuals. Proc Natl Acad Sci U S A 2001;98(18):10362–7.
[55] Dunn-Walters D, Townsend C, Sinclair E, Stewart A. Immunoglobulin gene analysis as a tool for investigating human immune responses. Immunol Rev 2018;284(1):132–47.
[56] Estes J, Baker JV, Brenchley JM, et al. Collagen deposition limits immune reconstitution in the gut. J Infect Dis 2008;198(4):456–64.
[57] Estes JD. Pathobiology of HIV/SIV-associated changes in secondary lymphoid tissues. Immunol Rev 2013;254(1):65–77.
[58] Li Q, Schacker T, Carlis J, Beilman G, Nguyen P, Haase AT. Functional genomic analysis of the response of HIV-1-infected lymphatic tissue to antiretroviral therapy. J Infect Dis 2004;189(4):572–82.
[59] Schacker TW, Nguyen PL, Martinez E, et al. Persistent abnormalities in lymphoid tissues of human immunodeficiency virus-infected patients successfully treated with highly active antiretroviral therapy. J Infect Dis 2002;186(8):1092–7.
[60] Keele BF, Tazi L, Gartner S, et al. Characterization of the follicular dendritic cell reservoir of human immunodeficiency virus type 1. J Virol 2008;82(11):5548–61.
[61] Lorenzo-Redondo R, Fryer HR, Bedford T, et al. Persistent HIV-1 replication maintains the tissue reservoir during therapy. Nature 2016;530(7588):51–6.
[62] Banga R, Procopio FA, Noto A, et al. PD-1(+) and follicular helper T cells are responsible for persistent HIV-1 transcription in treated aviremic individuals. Nat Med 2016;22(7):754–61.
[63] Estes JD, Kityo C, Ssali F, et al. Defining total-body AIDS-virus burden with implications for curative strategies. Nat Med 2017;23(11):1271–6.
[64] Rothenberger MK, Keele BF, Wietgrefe SW, et al. Large number of rebounding/founder HIV variants emerge from multifocal infection in lymphatic tissues after treatment interruption. Proc Natl Acad Sci U S A 2015;112(10):E1126–34.

[65] Vibholm LK, Lorenzi JCC, Pai JA, et al. Characterization of intact proviruses in blood and lymph node from HIV-infected individuals undergoing analytical treatment interruption. J Virol Apr 3 2019;93(8).
[66] Li Q, Lifson JD, Duan L, et al. Potential roles of follicular dendritic cell-associated osteopontin in lymphoid follicle pathology and repair and in B cell regulation in HIV-1 and SIV infection. J Infect Dis 2005;192(7):1269–76.
[67] Smith BA, Gartner S, Liu Y, et al. Persistence of infectious HIV on follicular dendritic cells. J Immunol 2001;166(1):690–6.
[68] Cavert W, Notermans DW, Staskus K, et al. Kinetics of response in lymphoid tissues to antiretroviral therapy of HIV-1 infection. Science (New York, NY) 1997;276(5314):960–4.
[69] Colomb F, Giron LB, Trbojevic-Akmacic I, Lauc G, Abdel-Mohsen M. Breaking the Glyco-code of HIV persistence and immunopathogenesis. Curr HIV/AIDS Rep Apr 2019;16(2):151–68.
[70] Ackerman ME, Crispin M, Yu X, et al. Natural variation in fc glycosylation of HIV-specific antibodies impacts antiviral activity. J Clin Invest 2013;123(5):2183–92.
[71] Kaneko Y, Nimmerjahn F, Ravetch JV. Anti-inflammatory activity of immunoglobulin G resulting from fc sialylation. Science (New York, NY) 2006;313(5787):670–3.
[72] Barouch DH, Stephenson KE, Borducchi EN, et al. Protective efficacy of a global HIV-1 mosaic vaccine against heterologous SHIV challenges in rhesus monkeys. Cell 2013;155(3):531–9.
[73] Bournazos S, Klein F, Pietzsch J, Seaman MS, Nussenzweig MC, Ravetch JV. Broadly neutralizing anti-HIV-1 antibodies require fc effector functions for in vivo activity. Cell 2014;158(6):1243–53.
[74] Forthal DN, Landucci G, Daar ES. Antibody from patients with acute human immunodeficiency virus (HIV) infection inhibits primary strains of HIV type 1 in the presence of natural-killer effector cells. J Virol 2001;75(15):6953–61.
[75] Hessell AJ, Hangartner L, Hunter M, et al. Fc receptor but not complement binding is important in antibody protection against HIV. Nature 2007;449(7158):101–4.
[76] Lofano G, Gorman MJ, Yousif AS, et al. Antigen-specific antibody Fc glycosylation enhances humoral immunity via the recruitment of complement. Sci Immunol 2018;3(26).
[77] Vadrevu SK, Trbojevic-Akmacic I, Kossenkov AV, et al. Frontline science: plasma and immunoglobulin G galactosylation associate with HIV persistence during antiretroviral therapy. J Leukoc Biol 2018;104(3):461–71.